Microporous and Mesoporous Materials 279 (2019) 61–72

Contents lists available at ScienceDirect

Microporous and Mesoporous Materials

journal homepage: www.elsevier.com/locate/micromeso

# A combined experimental and theoretical study on gas adsorption performance of amine and amide porous polymers

Ruh Ullah[a,1], Hasmukh Patel[b,1], Santiago Aparicio[c], Cafer T. Yavuz[d,**], Mert Atilhan[e,f,*]

[a] National Institute for Materials Science (NIMS), Japan
[b] Northwestern University, Evanston, USA
[c] Department of Chemistry, University of Burgos, Spain
[d] EEWS Graduate School, KAIST, Daejeon, Republic of Korea
[e] Department of Chemical Engineering, Texas A&M University, Qatar
[f] Gas and Fuels Research Center, Texas A&M University at College Station, USA

ARTICLE INFO

*Keywords:*
Covalent organic polymers
Gas adsorption
Density functional theory
Porous materials

ABSTRACT

In this manuscript, we report synthesis, characterization and application of amine and amide type covalent organic frameworks as $CO_2$ adsorbent materials at various isotherms and wide pressure conditions. Furthermore, we also report a detailed density functional theory investigation of the studied adsorbents in order to explain their adsorption behaviors and provide comparisons with experimental results. The objective of this work was to investigate custom design porous polymers by building amine and amide functionalities in the final structures, whether they have efficient $CO_2$ capturing performances at wide process conditions that covers both low and high pressure end applications to cover either pre- or post-combustion processes. On the other hand, energy storage performances of these materials were tested by performing $H_2$ sorption experiments as well. Two porous polymers, namely COP-9 and COP-10, were characterized with BET, TGA and FTIR to evaluate the physical properties of studied porous polymers and then were tested for $CO_2$, $N_2$ and $H_2$ adsorption both at low and high pressures. Studied materials were found to have compelling adsorption capacity mostly at high pressures and have very good selectivity for $CO_2/N_2$ and $CO_2/H_2$ respectively.

## 1. Introduction

The demand of more power production due to the technological development for the improvement of life style is increasing worldwide which in turn enhances the usage of fossil fuels and subsequently rising $CO_2$ emission and concentration in the environment [1–3]_ENREF_1. The renewal energy sources such as solar power, wind power, nuclear power and bio fuel power are still in the research and initial stages and consequently the world will have to depend mostly on fossil fuels for next few decades. It has been estimated that on average a single power plant using fossil fuels as power production source emits at least 3.5 million tons of $CO_2$ per year, whereas the number of such power generation industries increases globally [4]. Cement industries and transportation, which are the second and third major sources of $CO_2$ emission and environment pollution are also multiplying every year and accordingly enhancing the concentration of $CO_2$ in atmosphere [5]. Research has shown that the content of $CO_2$ in atmosphere may exceed 500 ppm by 2020 if not handle properly [6,7]. This alarming increase in $CO_2$ emission has severely threatened life on the earth and issues like global warming, severe weather conditions spread of very dangerous disease such as respiratory illnesses and asthma are all due to the excessive and uncontrollable emission of $CO_2$ [8–13].

The new energy production plants using fossil fuels however now changes to oxy-combustion fuel system and integrated gasification combine cycle system _ENREF_2 where $CO_2$ can be effectively captured using advanced technologies as well as mono-ethanol amine (MEA) as sorbent [8,14]. The cost of MEA regeneration, degradation, corrosive and toxic nature are still among the major challenges of the process industries that are dealing with $CO_2$ capture and mitigation [15].

Solid sorbents possess various advantages such as easier regeneration, reusability, environmental and economic viability, tunable capturing capacity and changeable selectivity [16]. Solid sorbents mainly have applications in pre-combustion system like IGCC, where, $CO_2$ can be separated from syngas after water shift in the process [14]. However,

* Corresponding author. Gas and Fuels Research Center, Texas A&M University at College Station, USA.
** Corresponding author.
*E-mail addresses:* yavuz@kaist.ac.kr (C.T. Yavuz), mert.atilhan@gmail.com (M. Atilhan).
[1] Equal Contribution.

https://doi.org/10.1016/j.micromeso.2018.12.011
Received 9 January 2018; Received in revised form 8 May 2018; Accepted 7 December 2018
Available online 12 December 2018
1387-1811/ 

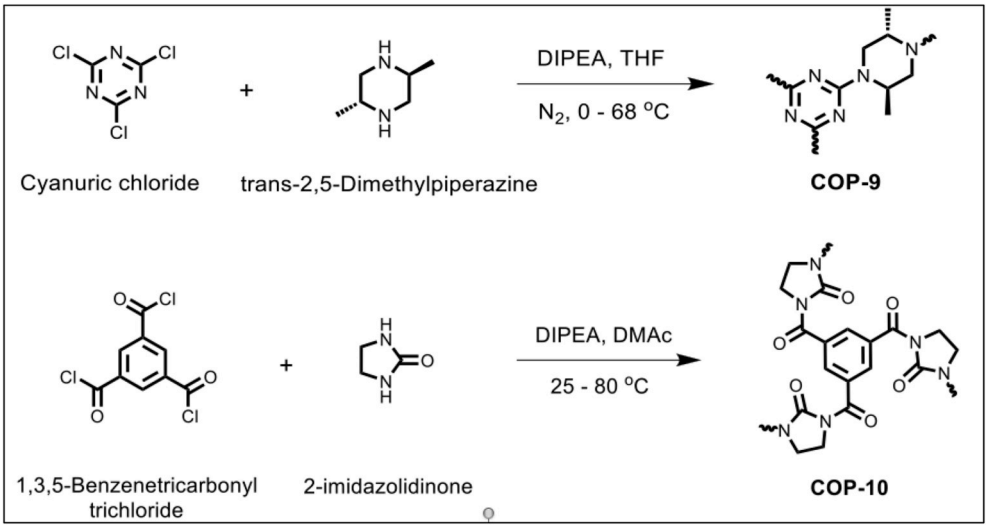


**Scheme 1.** Synthesis of COP-9 and COP-10.

this requires the adsorbents to be physically strong that can withstand high pressure and high temperature unlike the post-combustion process, where $CO_2$ can be separated at low pressures. In addition to the thermal and physical stability, solid sorbent needs to be selective for specific targeted gas (e.g. $CO_2$), high affinity for $CO_2$ and large pore volume for extended sorption performances. Various solid sorbents such as activated carbon, metal organic frameworks (MOFs) [17–20] _ENREF_3, zeolites [21–24], mesoporous silica (e.g. SBA-15) [25–27], nano-clays [28] and in the recent years many organic polymers have been investigated both for low and high-pressure $CO_2$ adsorption and separation purposes [16,27–35]_ENREF_11_ENREF_11. Attempts have been made to increase the $CO_2$ capturing capacity of solid materials by modifying their structure via inserting known high $CO_2$ affinity providing amine functional groups within the porous structure of adsorbents [36]. As an example SBA-15 has been impregnated with different function groups and tested for low and high pressure $CO_2$ adsorption [27]. Herein, we extend these efforts to COPs and report synthesis and characterization of COPs that can be assumed to be the more favorable compounds as long as the affinity of $CO_2$ and the capturing capacity of solid sorbents is concern at high pressure [27,37–39]. Two COPs materials are reported that are produced by using different building block monomers and linked with two different linkers to investigate the effect of different functionality on the gas sorption (mainly $CO_2$) at low and high pressures at different isotherms.

## 2. Experimental

### 2.1. Materials and synthesis procedure

In this work, two COPs are reported and they are named as COP-9 and COP-10 (numbering is based on ongoing study of developing an inventory of new COPs based on the core monomer and linker selections). N,N-Diisopropylethylamine, 1,3,5-benzene tricarbonyltrichloride, 2,5-Dimethylpiperazine, cyanuric chloride, 2-imidazolidinone, dimethylacetamide, and tetrahydrofuran (THF), purchased from Sigma-Aldrich, however, dioxane and ethanol were obtained from TCI, Japan. All the chemicals were used without any further modification and/or dilution. COP-9 and COP-10 were prepared through the following procedures.

In a typical procedure N,N-Diisopropylethylamine (1.9 mL, 10.8 mmol) was added to trans-2,5-Dimethylpiperazine (0.48 g, 4.2 mmol) dissolved in THF _ENREF_4 at 0–5 °C. Cyanuric chloride (0.5 g, 2.7 mmol) dissolved in THF _ENREF_5was added dropwise to the above solution with continuous stirring at 0–5 °C in $N_2$ environment. The solution was stirred at 0–5 °C for 1 h. Subsequently, the temperature of the reaction mixture increased to 25–30 °C and stirred for 2 h, followed by heating at 68–70 °C for 21 h. The precipitate was washed with THF, dioxane and ethanol (three times each). Finally, the precipitate was dried at room temperature for 2 h and 80–90 °C for 5 h under vacuum and labeled as COP-9.

N,N-Diisopropylethylamine (2.1 mL, 12 mmol) was added to 2-imidazolidinone (0.4 g, 4.65 mmol) dissolved in Dimethylacetamide (DMAc, 35 mL) at 25 °C. 1,3,5-Benzenetricarbonyl trichloride (0.8 g, 3 mmol) dissolved in DMAc (25 mL) was added dropwise to the above solution with continuous stirring at 25 °C. The solution was stirred at 25 °C for 2 h. Subsequently, the temperature of the reaction mixture increased to 80 °C and stirred for 16 h. The reaction mixture cooled to room temperature and 250 mL of de-ionized water added which resulted precipitate. The precipitate was washed with water and ethanol (three times each) and it was dried at room temperature for 2 h and 80–90 °C for 5 h under vacuum and labeled as COP-10. Structures of both COP-9 and COP-10 are shown in Scheme 1.

### 2.2. Characterization and sorption experiments

Thermal stability of COP-9 and COP-10 was conducted with Perkin Elmer Pyris 6 (Thermogravimetric Analysis) TGA model 4000 system. TGA system was properly balanced and calibrated according to the purging gas ($N_2$), crucible and sample holder stem. TGA machine was equipped with chiller from Huber model Pilot One to automatically maintain the temperature of the system and $N_2$ was used in the heating environment, where the materials were heated directly from 30 °C to 800 °C at the rate of 1 °C per minute. Physical parameters such as pore volume and surface area of materials were estimated using Brunauer-Emmett-Teller (BET) analyzer Model micrometrics ASAP 2420. The solid materials were vacuumed for 24 h prior to the BET measurements in order to avoid any blockage of pore with moisture. FTIR measurements were carried out by using Bruker® Vertex 80 Fourier transform infrared spectrometer.

Two different apparatus were used for the sorption measurements. For low-pressure measurements Setaram (PCT Pro) apparatus and for the high-pressure measurements Rubotherm Magnetic Suspension Sorption Balance (MSB) was used. PCT Pro is equipment, which determines the gas sorption properties of both solid and liquid at various temperatures and pressures based on the volumetric measurement method and the details of the working principle of this apparatus is provided in the Electronic Supporting Information (ESI) section of this manuscript. MSB apparatus used well-established gravimetric method for sorption experiments. The apparatus is equipped with automated Teledyne Isco260D pump was used to measure the high-pressure gases

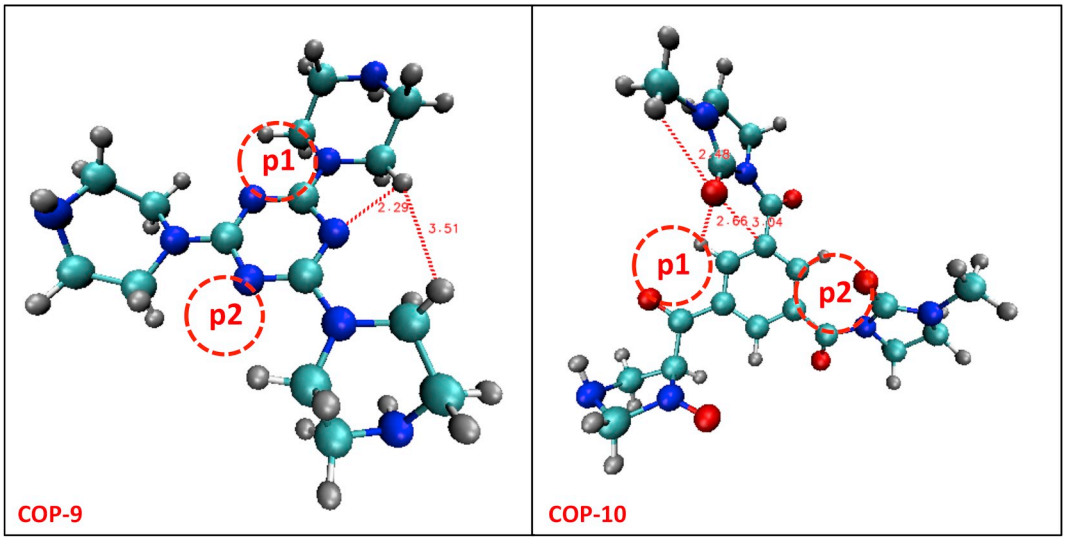


**Scheme 2.** Final geometry of structures optimized with B3LYP 6–311 + + G** theory level. (a) COP-9 and (b) COP-10. Positions p1 and p2 are displayed, where $CO_2$ and $N_2$ are placed around the core molecule and near ligand molecule in COP structure during the DFT simulations.

uptake by materials. Details experimental set up of MSB for high pressure gases measurement has been mentioned in literature [40] and some further details of the working principle of this apparatus is also provided in ESI.

### 2.3. Theoretical

A detailed DFT analysis were carried out for the studied COP structures for their interactions with $CO_2$ and $N_2$ alone as well as and $CO_2/N_2$ existing together around the COP structures. Scheme 2 shows the different $CO_2$ and $N_2$ spatial positions based on the to infer interaction properties at all logical active sites of the COP molecules (e.g. p1, p2 positions for $CO_2$ and $N_2$).

Initial structures were built by Avogadro software [41]. DFT calculations were carried out with the ORCA program [42]. All the calculations were done with the B3LYP functional [43,44] together with the DFT-D3 method by Grimme [45], for considering dispersion interactions, and the 6–311 + + G** basis set (B3LYP/6–311 + + G** theoretical level). The quantum theory of atoms in molecules (AIM) has been widely used to analyze the real space functions and characterize the type of different interactions. The topology of COP9/10-$CO_2/N_2$ interactions were analyzed according to the Bader's AIM theory [46], using the Multiwfn code [47]. Intermolecular interactions are characterized by the formation of several bond critical points (BCPs), accompanied by ring critical points (RCPs) at the center of the interaction region. Likewise, BCPs between COP molecules and $CO_2/N_2$ are characterized by the values of electron density, ρ, and Laplacian of electron density, $\nabla^2\rho$. Analyzed topological values for AIM and BCP are given in Table S1. On the other hand, RDG has been used for developing gradient-corrected functional of increasing quality [48–50]. By this method both nature and strength of the interactions are displayed in isosurface. This latter method of RDG is used in this study for studying the strength and the interaction types of COP structures visually through the analysis of the calculated isosurfaces.

## 3. Results and discussions

### 3.1. Experimental

Thermal gravimetric analysis of both COP-9 and COP-10 (shown in Figure S1) reveals that COP-9 is thermally more stable than COP-10, since; the former is almost stable up to 400 °C. TGA further indicates that COP-10 is thermally degraded in three steps, while COP-9 decomposes in two steps. The initial degradation of COP-10 starts at around 75 °C which can be associated to the evaporation of stored water within the structure, 2nd degradation of COP-10 starts at around 200 °C, while the third one starts at 400 °C. Contrary, COP-9 is about completely stable up to 400 °C however, beyond this point it decomposed quickly and in another 100 °C increase in temperature, almost 50% of the material losses. TGA analysis confirmed that COP-9 is much stable than COP-10, however, it degrades gradually while a sharp degradation in COP-9 can be observed after 400 °C.

Physical properties and proposed chemical structure of COPs are given in Table 1, which shows that COP-9 has smaller pore volume than COP-10, however, the former has larger surface area and lower tapped bulk density. It has been assumed that low pressure gases uptake by solid materials is mostly governed by the physical parameters such as pore volume and surface area [51]. On the other hand adsorption capacity at high pressure does not necessarily depend upon the porosity of the structure. Porosity of the material is certainly one of the most important parameter that determines the sorption performance, however, affinity of the materials can dramatically enhance the sorption performance if the sorbent structure is carefully tailor made for a specific purpose. Thus the material with lower porosity and lower surface area may have higher affinity at high pressure and thus it might have high $CO_2$ (or any other gas) sorption performance at elevated pressures when compared to those adsorbents that have larger physical parameters [52,53].

Moreover, nitrogen adsorption and desorption isotherm at 77 K and BJH pore size distribution patterns that are calculated from desorption isotherm data for COP–9 and COP–10 are provided in Figure S2, and

**Table 1**
Physical Parameters and structure of covalent organic polymers (COPs).

| Sample Code | Structure | Surface area ($m^2/g$) | | Pore volume ($cm^3/g$) | Density ($cm^3/g$) | |
|---|---|---|---|---|---|---|
| | | BET | Langmuir | | Bulk | Tapped |
| COP-9 | 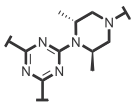 | 146.4 | 204.3 | 0.244 | 0.181 | 0.202 |
| COP-10 | 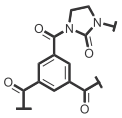 | 84.5 | 114.6 | 0.634 | 0.129 | 0.258 |

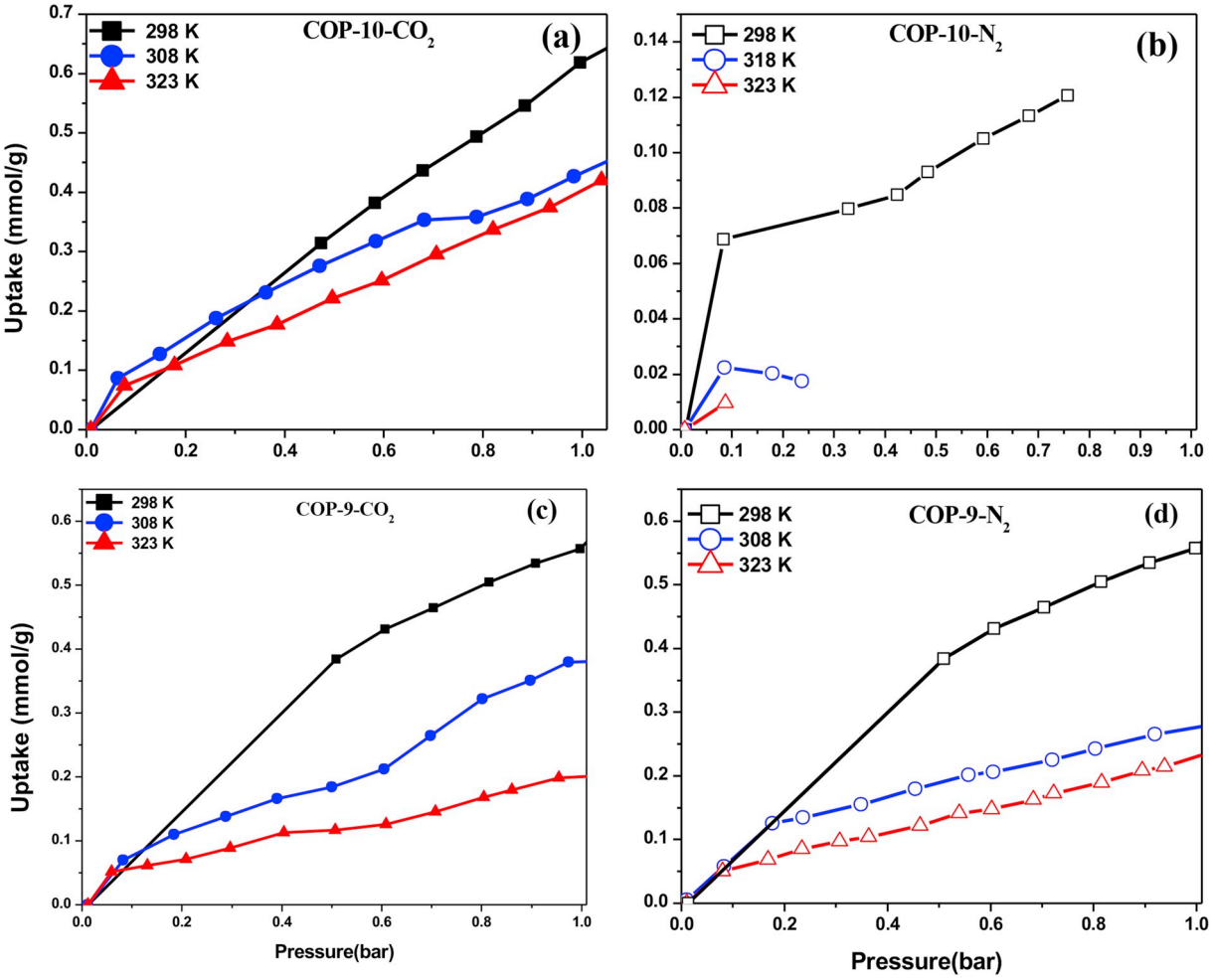


**Fig. 1.** $CO_2$ and $N_2$ adsorption of COP-9 (c & d) and COP-10 (a & b) at maximum of 1 bar and three different isotherms obtained with PCT-Pro apparatus.

BET linear plot from $N_2$ adsorption at 77 K for COP–9 and COP–10 are provided in Figure S3.

FTIR analysis in Figure S4 shows the formation of amine and amide COPs. Observed noticeable peaks are 1240 $cm^{-1}$, 2974 $cm^{-1}$ for COP-9 represents C—N asymmetric stretch and C—H symmetric stretch for piperazine linker respectively. Moreover, little shoulder at 1281 $cm^{-1}$, two peaks at 1178 $cm^{-1}$ and 1343 $cm^{-1}$ represent amine structure C—N stretching for COP-9. For COP-10 1670 $cm^{-1}$ represent typical saturated amide (6 atom ring) C = O stretching, 1370 $cm^{-1}$ represent $sp^3$ C—N single bond stretch respectively [54]. The broad band around 3623–3731 $cm^{-1}$ is mainly a combination of trapped moisture in the pores. Other peaks can be observed from figure S4 in ESI.

Fig. 1, shows the low pressure $CO_2$ and $N_2$ adsorption of COP-9 and COP-10, which clearly indicates that COP-10 captures comparatively more $CO_2$ at lower pressure of 1 bar due to the larger pore volume. Xiang et al. reported that COP-1 possess the highest surface area captured more $N_2$ and $CH_4$; however, COP-2 with larger pore volume captured more $CO_2$ and $H_2$ than all other organic polymers [55] (Scheme 3).

On the other hand COP-10 uptakes very low quantity of $N_2$ at 1 bar and three different temperatures as compared to COP-9. It must be noted that selectivity of COP-10 for $CO_2$:$N_2$ at low pressure is much higher than that of COP-9. Additionally as given in Table 2, selectivity of COP-10 for $CO_2$:$N_2$:$H_2$ is also better than that of COP-9 at 308 K, while at all other temperatures selectivity of both polymers is similar. Selectivity values that are reported in Table 2 are based normalized values that are obtained through single gas sorption experiments.

Additionally, the selectivity of COP-10 at atmospheric pressure is

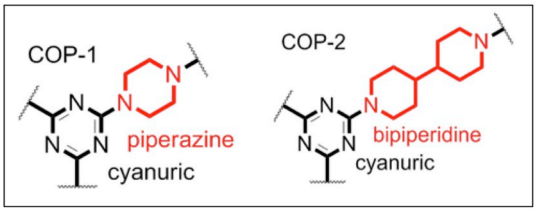


**Scheme 3.** Structures for COP-1 and COP-2.

increasing with rising temperature and becomes infinity at temperature above than 308 K. As shown in Fig. 1b COP-10 is totally inert for $N_2$ at higher temperatures, although it captures a bit smaller quantity of $N_2$ at standard temperature and pressure. Fig. 1c and d indicates that COP-9 uptake less $CO_2$ than COP-10, but its $N_2$ uptake is comparatively larger than that of COP-10. Table 2 indicates that the overall performance of COP-10 at atmospheric pressure and different temperatures is comparatively better than COP-9, since the former adsorb more $CO_2$ and less $N_2$ which makes this material favorable for the pre-combustion $CO_2$ capture and separation.

Fig. 2 shows $CO_2$ and $N_2$ uptake capacity of COP-9 and COP-10 at maximum pressure of 200 bars at three different isotherms. Fig. 2a and c compares the $CO_2$ uptake capacity of COP-9 and COP-10 up to 200 bars. Automated MSB system handles the pressurizing and depressurizing sequence as per the initial determination of the pressure points for each isotherm. Since the high-pressure measurements require higher equilibration time for both pressure and temperature, pressurizing and depressurizing sequence has been carefully executed for the MSB

**Table 2**
Maximum gases ($CO_2$, $N_2$ and $H_2$) uptake capacity of COP-9 and COP-10 at atmospheric pressure, high pressure of 200 bars and three different temperatures.

| Gas | $CO_2$ (mmol/g) | | | $N_2$ (mmol/g) | | | $H_2$ (mmol/g) | | | Selectivity ($CO_2$:$N_2$:$H_2$) | | | |
|---|---|---|---|---|---|---|---|---|---|---|---|---|---|
| Temp. (K) | 308 | 323 | 338 | 308 | 323 | 338 | 308 | 323 | 338 | 308 | 323 | 338 | **200 bar** |
| COP-9 | 79 | 70 | 64 | 21 | 19 | 17 | 10 | 9 | 8 | 8:2:1 | 8:2:1 | 8:2:1 | |
| COP-10 | 52 | 42 | 38 | 12 | 11 | 9 | 5.6 | 5.1 | 4.7 | 9:2:1 | 8:2:1 | 8:2:1 | |

| Gas | $CO_2$ (mmol/g) | | | $N_2$ (mmol/g) | | | Selectivity ($CO_2$:$N_2$) | | | |
|---|---|---|---|---|---|---|---|---|---|---|
| Temp. (K) | 298 | 308 | 308 | 298 | 308 | 323 | 298 | 308 | 323 | **1 bar** |
| COP-9 | 0.6 | 0.38 | 0.2 | 0.6 | 0.3 | 0.2 | 1:1 | 1:1 | 1:1 | |
| COP-10 | 0.7 | 0.5 | 0.42 | 0.12 | 0.02 | 0.00 | 6:1 | 25:1 | ∞ | |

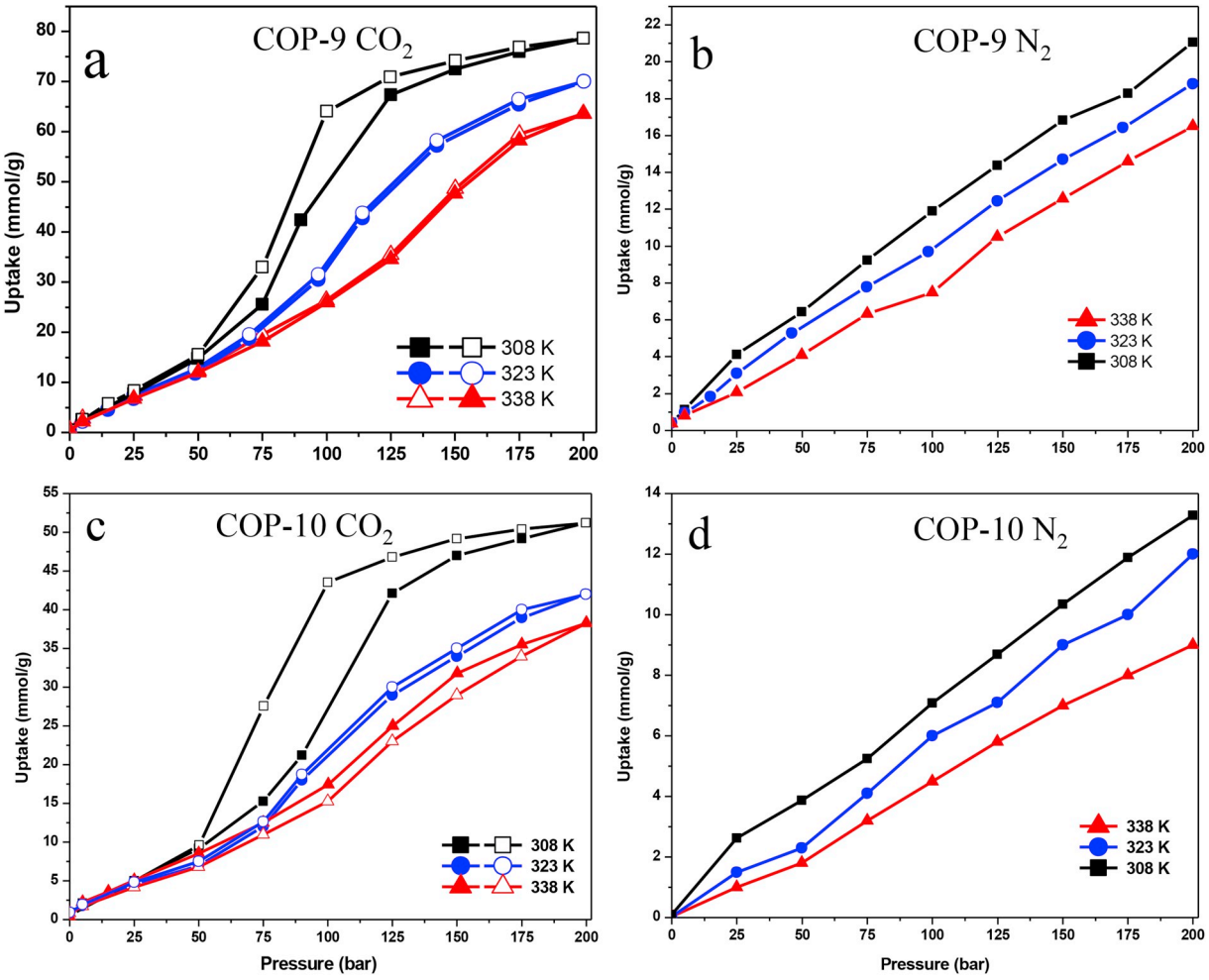


**Fig. 2.** $CO_2$ and $N_2$ adsorption of COP-9 (a & b) and COP-10 (c & d) at maximum of 200 bar and three different temperatures obtained with magnetic suspension balance (MSB). Full symbols show adsorption and empty symbols shows desorption.

experiments. Once the MSB system reaches the highest set pressure points determined for the experiments, pressure of the apparatus was gradually reduced until it reaches to the next experimental pressure point and stays there until temperature and pressure equilibrium is observed (typically 45 min for adsorbent systems). Once the gas adsorption at set pressure point is completed, then the system is brought to the next pressure point, and this operation continues until the collection of the vacuum measurement as a last experimental point of the isotherm. The gas sorption system is fully automated and the pressure goes to next higher point after completing the previous measurement point. As mentioned, the system was brought to vacuum measurement and then final vacuum (approximately for 8 h) at the same isotherm. This explained measurement routine was repeated for both COP-9 and COP-10 samples at each isotherms. Fig. 2 reveals that unlike low pressure capturing capacity, COP-9 uptakes more $CO_2$ than COP-10 at three temperatures. Further details of the MSB working principles are explained in our previous works in which similar porous structures were experimented [34,56–60]. It is important to note that the pore volume of COP-10 is considerably larger than COP-9, but the later has more $CO_2$ capture capacity at higher pressures. Surface chemistry and the pore size are the two main factors that determine the adsorption performance. Affinity between the active site of the adsorbent and the gas molecules dominates the adsorption process at lower pressures. Regardless of the affinity, at higher pressures the gas adsorption amount is strongly correlated with the pore volume. Considering adsorption performances of the two studied COPs at low and high pressures, the possibility of structural rearrangement of COP-10 at higher pressures (linker length argument proposed above) could have resulted in a much lower pore volume and thus lower gas uptake than COP-9.

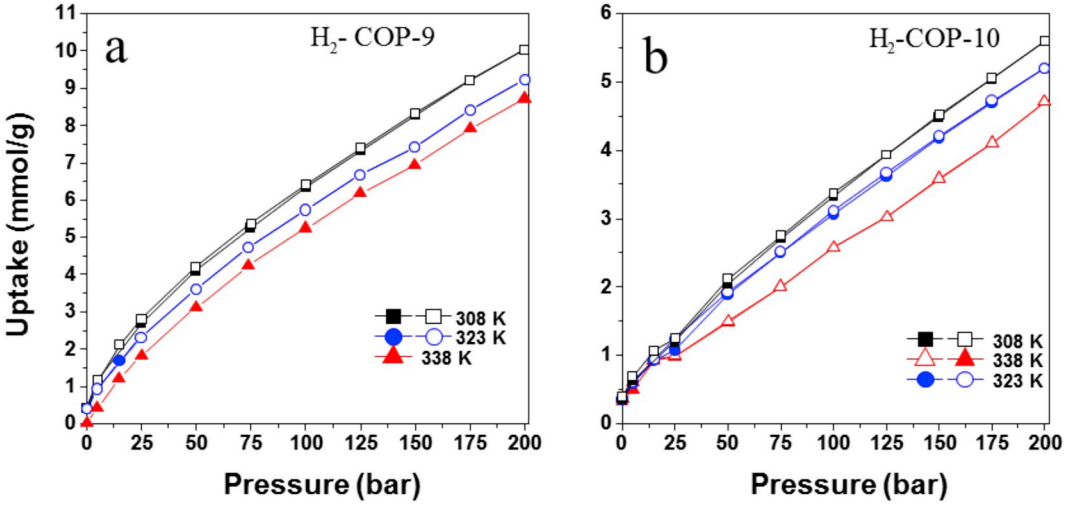


**Fig. 3.** $H_2$ adsorption-desorption isotherms of COP-9 (a) and COP-10 (b) at maximum of 200 bar and three different temperatures obtained with magnetic suspension balance (MSB). Full symbols show adsorption and empty symbols shows desorption.

In addition to the effect of pore volume and surface area on the gases uptake capacity of solid sorbents, from nanoscopic approach point of view the affinity of the gas molecules toward the attractive sites also contribute to the adsorption capacity of materials. It can be assumed that COP-9 has more compelling interacting sites than COP-10 since the core monomer of COP-9 has three nitrogen nodes whereas the core monomer of COP-10 has less. On the other hand, COP-10 has more −OH functional groups, which has less affinity for $CO_2$ than the −NH functionality [61]. Three −NH groups in the starting material cyanuric chloride increases the $CO_2$ affinity of COP-9 in comparison to COP-10, which is composed of carbonyl (C=O) group, due to the reason that −N functionality in the core structure of polymers may make this material more attractive for $CO_2$ capture than any other material [61,62]. As a summary, it can be argued that, although COP-9 has lower pore volume that was calculated at low pressure, enhanced $CO_2$ adsorption performance of COP-9 could be directly related primarily to the structural transformations and rearrangements through to the flexible linker structures. Furthermore, more and stronger active sites for $CO_2$ might have played a secondary role on adsorption performance as well, which could not show a dominant effect against the pore volume at low pressures. Therefore, we can argue that despite higher gas affinity for a particular porous material, pore volume dominates the adsorption performance since the adsorption deals with the amount of adsorbate that can be stuffed in a pore.

Fig. 2 also compares the $CO_2$ and $N_2$ adsorption capacity of COP-9, which reveals that it captures 4 times more $CO_2$ than $N_2$. Isotherms of $CO_2$ are showing typical type IV behavior [63], while isotherms of $N_2$ are not resembling to any specific sorption isotherm behavior but gradually increasing with increase in pressure. A slight hysteresis behavior at the adsorption/desorption cycle is observed for $CO_2$ isotherms for both COP-9 and COP-10, which is more prominent at 308 K isotherm as compared to that obtained at higher temperatures. Typically, the hysteresis starts at around 50 bars and expands further with till 125 bars, beyond which the hysteresis disappears and adsorption/desorption occurs on the same path. This phenomenon of the hysteresis in both the materials, which is more visible in COP-10, can be attributed to the microporosity and mesoporosity of these structures. Moreover, hysteresis behavior is observed to be higher and more visible at lower isotherms and cause higher amount of uptake capacity, which is an indication of a potential tendency on the materials towards swelling behavior. In order to study the origins of hysteresis observation require further more in depth analysis with the quantification of the swelling effect and through detailed nanoscopic behavior study, and authors are working on this by using nanoscopic approach (e.g. DFT and MD). It is of worth mentioning here that although hysteresis exists in the isotherms of $CO_2$ at a pressure range of 50–175 bars but the adsorption-desorption curves completely overlaps at the lower pressure. This clearly shows that both the COP-9 and COP-10 can be entirely evacuated after releasing the pressure and no $CO_2$ molecule was chemically bonded to the COPs structures.

This behavior of perfectly physical adsorption of $CO_2$ and $N_2$ makes these materials more compelling since these compounds can be repeatedly used and regenerated easily without extra expenses and efforts. Importantly, $CO_2$ and $N_2$ were alternatively subjected to these materials at various temperatures to check the repeated applications of these compounds under various temperature and pressures conditions. All studied COPs were exposed to cyclic (at least 3 cycles per each sample) adsorption/desorption experiments for observing the activity and performance of the materials, and no significant degradation on the sorption activity of the COPs were observed. Another important and yet expected feature of these compounds was the trend of decrease in the adsorption capacity with increase in temperatures, since in both cases of $CO_2$ and $N_2$ the maximum adsorption capacity was less at higher temperature than at lower temperature. This is because of the exothermic effect of the adsorption-desorption process.

Integrated gasification combine cycle system requires pre-combustion $CO_2$ separation from $H_2$ at elevated temperature and pressure after the water-gas shift reaction. Solid membranes and adsorbents have been considered as more advantageous than liquid scrubbers in the pre-combustion capture system due to the regeneration and multiple applications of the sorbents. In order to further investigate the possible consideration and applications of COP-9 and COP-10 in pre-combustion $CO_2$ capture, these materials were also tested for hydrogen adsorption at high pressure and high temperature. The data obtained for $H_2$ uptake of these two polymers at different conditions is given in Table 2. Fig. 3 also compares $H_2$ uptake capacity of both the materials measured at similar pressure and temperature conditions as used for $CO_2$ and $N_2$ adsorption. It is evident from Fig. 3a that COP-9 uptakes almost double quantity of $H_2$ than COP-10 (Fig. 3b). Although, COP-9 uptakes large quantity of $CO_2$ at high-pressure, however, selectivity of COP-10 both for $CO_2$:$N_2$ at lower pressure and for $CO_2$:$N_2$:$H_2$ at high pressure is comparatively better than the former. As shown in Table 2, the normalized single gas selectivity values of both the COPs at high pressure is almost same at all the temperatures, which reveals that temperature modification is not important for the selectivity of materials. On the hand at lower pressure selectivity of COP-9 is unchanged with respect to temperature while selectivity of COP-10 is significantly varies with temperature and at higher temperature COP-10 becomes almost $N_2$

**Table 3**
Comparison of COPs that are synthesized by using amine and amide based linkers and COPs that are presented in this work.

| COP No. | Core | Linker Group | Linker Specific | $CO_2$ Sorption [mmol/g] | | $N_2$ Sorption [mmol/g] | | BET | | Ref. |
|---|---|---|---|---|---|---|---|---|---|---|
| | | | | | | | | Surface Area | Pore Vol. | |
| | | | | 200 bar 308 K | 1 bar 298 K | 200 bar 308 K | 1 bar 298 K | [$m^2$/g] | [$m^3$/g] | |
| COP-1 | cynanuric chloride | Amine | piperazine | 128 | 1.36 | – | 0.086 | 168 | 0.25 | Ref. [58] |
| COP-9 | | | trans-2,6-dimethylpiperazine | 79 | 0.60 | 21 | 0.600 | 146 | 0.24 | This Work |
| COP-2 | | | bipiperadine | 47 | 0.93 | – | 0.186 | 158 | 0.67 | Ref. [58] |
| COP-33 | 1-3-5 benzenetricarbonyl | Amide | 1,4-phenylenediamine | 133 | 0.60 | 30 | 0.020 | 53 | 0.20 | Ref. [34] |
| COP-32 | trichloride | | 4-aminobenzylamine | 128 | 0.44 | 31 | 0.020 | 46 | 0.14 | Ref. [34] |
| COP-34 | | | 1,3-phenylenediamine | 63 | 0.47 | 15 | 0.025 | 33 | 0.10 | Ref. [34] |
| COP-10 | | | 2-imidazolidinone | 52 | 0.70 | 12 | 0.120 | 85 | 0.63 | This Work |

phobic in the case of $CO_2$ and $N_2$ selectivity comparison. Upon comparing the $CO_2$ adsorption capacities of COP-9 and COP-10 to that of other similar porous organic polymer networks in literature such as PPN-4, PAF-1, polybenzimidazoles and some other COPs [64], it can be seen that COP-9 has better performance when the $CO_2$ capture capacity (82 mmol/g at 308 K) is considered [60,64].

On the other hand, some other previously published COPs that uses similar core polymer compound as well as similar linker groups [34,57]. A detailed comparison for COPs that uses cynanuric chloride and 1-3-5 benzenetricarbonyl trichloride as polymer core that are combined with amine and amide based linkers are provided in Table 3.

Amongst the published COPs that uses amine based linkers, COP-1 that uses piperazine showed superior $CO_2$ capture performance (128 mmol $CO_2$/g of sample) at high pressures in comparison with COP-9 (79 mmol $CO_2$/g of sample) that uses trans-2,6-dimethylpiperazine as linker. Whereas, COP-9 has showed almost twice as better CO2 capture performance than COP-2 at high pressures (47 mmol $CO_2$/g of sample) that uses bipiperidine as linker element. However, while COP-1 has massive 1.36 mmol $CO_2$/g of sample, unlike performance comparison at high pressures COP-2 has shown superior performance (0.93 mmol $CO_2$/g of sample) in comparison to COP-9 (0.60 mmol $CO_2$/g of sample) at 1 bar and 298 K that makes is more suitable at post combustion process conditions [65]. Although COP-2 has slightly higher surface area than that of COP-9, higher amount of internal molecular free volume might possibly lead to some "hidden" micropores for $CO_2$ to permeate in the COP. Moreover, lower $CO_2$ adsorption capacity of COP-2 despite their relatively higher measured BET surface area can be explained by the large percentage of mesopores in COP-2, which leads increase in the surface area but does not necessarily benefit the $CO_2$ capture capacity performance. These results show that the affinity of $CO_2$ and gas sorption performance can be adjusted by manipulating the linker type that leads to changes in pore size and pore volume of the COPs, and plays a decisive role on the sorption capacity more than surface area. When the linkers are considered, the length of piperazine is shorter than the length of the trans-2,6-dimethylpiperazine and that is shorter than the length of bipiperadine. In can be seen that the $CO_2$ uptake performance of the compared COPs that are prepared with shorter linker had higher than their analogues with long linker. The linkers that are used in COP-1-2-9 are all serve for the purpose of pressure triggered flexible structure and performs better under high-pressure conditions, which make them more suitable for pre-combustion type applications.

When amide based COPs are considered, based on the $CO_2$ capture performances following order has been observed: COP-33 > COP-32 > COP-34 > COP-10 based on the sorption values reported at 200 bars and at 308 K isotherm [34]. However at low-pressure conditions at 1 bar and at 298 K isotherm, COP-10 has showed the best $CO_2$ sorption performance amongst the other COPs that use amide based linkers. The final structure and porous structure of the COPs can be tailored by alternating the type (e.g. length) of the linkers and type of starting core building blocks (e.g. cyanuric chloride or 1-3-5 benzenetricarbonyl trichloride). Shorter linkers can lead to COPs with better microporosity, whereas longer linkers prove to hinder the microporosity due disruptions within the covalent organic framework. Flexibility of the final COP structure also plays a crucial role in the gas storage and sorption performance at elevated pressures [66]. Considering these facts, despite highest obtained surface area amongst the amide based COPs listed in Table 3, due to its high pore volume COP-10 lead to higher $CO_2$ sorption performance at low pressures. Meanwhile, due to the longer and more flexible linker properties, COPs-32-33-34 showed better performance at higher pressures.

As an essential property for making benchmarking decision on sorbent performance for a adsorption-desorption process is the rate of adsorption and it was calculated via mathematical expression mentioned in literature [9] in the term of mass transfer coefficient k (1/sec) (shown in Fig. 4), which is displayed at both isotherms. COP-9 comparatively adsorbed more $CO_2$ than COP-10, and also its rate of adsorption is higher than COP-10 at both isotherms. Additionally, Fig. 4 show that at 308 K COP-9 has the highest $CO_2$ capture rate of $112 \times 10^{-4}$ $sec^{-1}$. It is observed that rate of adsorption reduces at higher isotherms, however, in case of COP-10, pressures that are higher than 70 bar, relative adsorption rate at 323 K becomes quicker than the case of 308 K. As Boa et al. explained [67], in some cases adsorption of $CO_2$ can be quicker and thus the adsorption equilibrium can be achieved rapidly at higher isotherms. Unlike to Brownian motion of gases, decrease in the adsorption rate on the adsorbent surfaces and within the pores is due the exothermic nature of the adsorption process, which deters the adsorption capacity on the surfaces. The gas-solid interface, hydrogen bonding and Van der Waal forces between adsorbate and adsorbent restrict the mass transfer coefficient of $CO_2$ adsorption on the COPs. Moreover, surface heterogeneity is one of the other factors that have an important role in the adsorption process, which may leads to the enhancement in the heat of adsorption and to the reduction in the adsorption rate.

Gas adsorption on a porous material is an exothermic process in which heat is released [39], and heat of adsorption (shown in Fig. 5) for each material at both isotherms were calculated by applying Clapeyron equation at particular number moles of $CO_2$ captured by the adsorbents [68]. As shown in Fig. 5, the material with largest adsorption quantity COP-9 has highest heat of adsorption, which decreases with increasing the number of adsorbed mole on the materials surfaces. COP-9 has the highest heat of adsorption when compared with COP-10, which is similar to the adsorption trend of $CO_2$ as given in Fig. 2.

### 3.2. DFT results

Geometry of COP-9 and COP-10 compounds were optimized at B3LYP 6–311 + +G** theory level and the final structures are given in

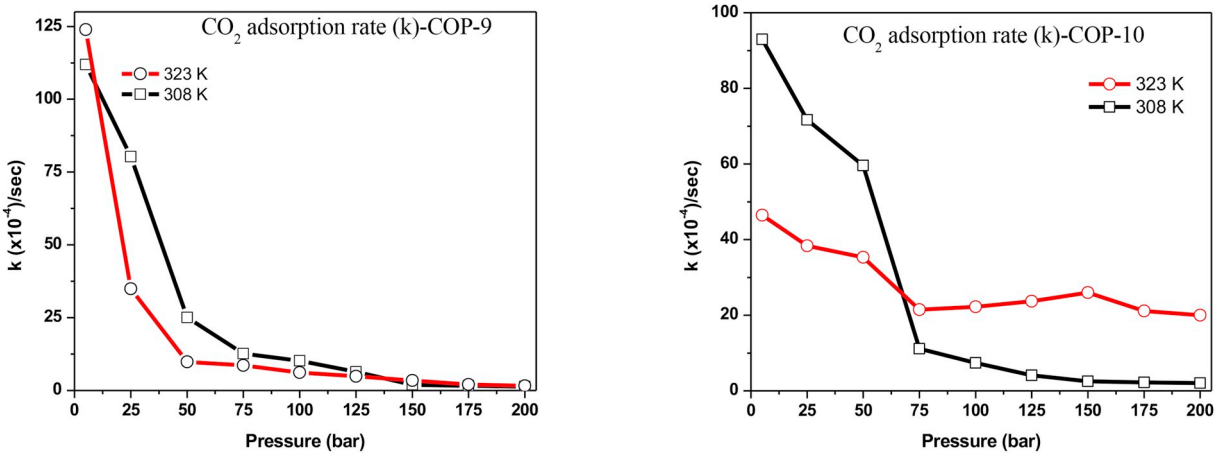


**Fig. 4.** Rate of adsorption calculated from data of $CO_2$ adsorption at for COP-9 and COP-10.

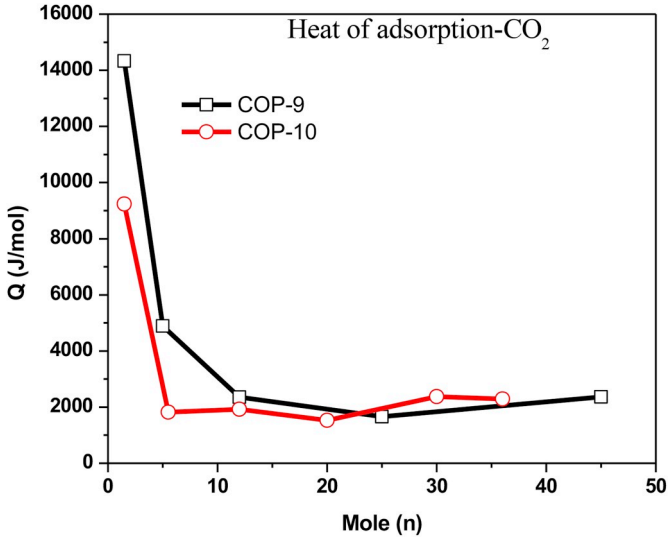


**Fig. 5.** Heat of adsorption associated with $CO_2$ adsorption for COP-9 and COP-10.

Scheme 2 for both COPs. The reason for the DFT study and relevant calculations is to provide detailed explanation on the type and strength of interaction between the porous material and the gas molecules at molecular level. The explanation or interpretation of the experimental results with DFT calculation results is not possible with straightforward approach. DFT results can only provide insights on the interaction mechanism by quantifying and visualizing the obtained simulation results. In order to mimic the adsorption process in bulk, further detailed molecular dynamic simulations are required, which is not the focus of this study. Having mentioned the aim of the DFT studies of this work, we analyzed the characteristics of bonding type and strength for COP materials in the case of $CO_2/N_2$ in close proximity of COP adsorption sites and used these simulation results to suggest further explanations to experimental findings. Figs. 6 and 7 show both AIM and RDG analysis of COP-9 interaction with $CO_2$ and Figs. 8 and 9 present the same information for COP-10. Numerical data for BCPs that were calculated according to Bader's theory [46], ρ and $\nabla^2\rho$ for all studied DFT cases are provided in Table S1. One shall keep in mind the definition of hydrogen bonding according to AIM theory stands that ρ and $\nabla^2\rho$ must be in the range 0.002–0.04 a.u. and 0.020 to 0.139 a.u, respectively [69] while analyzing the presented results herein.

When BCPs for COP-9 – $CO_2$ interaction are considered for both p1 and p2 positions, it was noticed that COP-9-p1 at BCP#2 has highest values of ρ and $\nabla^2\rho$ amongst the other studied cases for COP-9 with 0.00074762 a.u. and 0.013382 a.u. respectively. COP-9-p1 at BCP#2 points out high C···N interaction of $CO_2$ and COP-9. On the other hand, for COP-9 – $N_2$ interactions, COP-9-N-p1 at BCP#1 has resulted with highest values of ρ and $\nabla^2\rho$ values with 0.00011455 a.u. and 0.0012619 a.u. respectively, which shows interaction between N···C(H) of the COP-9 linker. Moreover, $CO_2$ and $N_2$ BCP values show superior $CO_2$ interaction in comparison with the $N_2$ interactions, which was observed experimentally as well.

In the case of BCPs analysis for COP-10 – $CO_2$ interactions, it was calculated that COP-10-p2 at BCP#2 has highest values of ρ and $\nabla^2\rho$ amongst the other studied cases for COP-10 with 0.00151103 a.u. and 0.0337295 a.u. respectively. This interaction takes place at C···O—C sites according to Fig. 8. On the other hand, for COP-10 – $N_2$ interactions, COP-10-N-p1 at BCP#1 has resulted with highest values of ρ and $\nabla^2\rho$ values with 0.00057561 a.u. and 0.0113955 a.u. respectively, which shows interaction between N···O—C of the COP-10 linker. Moreover, $CO_2$ and $N_2$ BCP values show superior $CO_2$ interaction in comparison with the $N_2$ interactions, which was observed experimentally as well.

We also compared the BCP values for $CO_2$ for both the COPs, and the results for COP-10-C-p2 at BCP#2 is higher than that of the BCP value at BCP#2 for COP-9-p1. This result coincides with the "low-pressure" adsorption experimental data that is given in Fig. 1. However, the quantification of the AIM results doesn't agree with the high-pressure adsorption values (Fig. 2) and this was previously explained as the $CO_2$ uptake performance of COPs with shorter linker had higher than their analogues with long linker. The linker that was used in COP-9 serves for the purpose of pressure triggered flexible structure and performs better under high-pressure conditions. Surface chemistry and the pore size are the two main factors that determine the adsorption performance. Affinity between the active site of the adsorbent and the gas molecules dominates the adsorption process at lower pressures. Regardless of the affinity, at higher pressures the gas adsorption amount is strongly correlated with the pore volume. Considering adsorption performances of the two studied COPs at low and high pressures, the possibility of structural rearrangement of COP-10 at higher pressures (linker length argument proposed above) could have resulted in a much lower pore volume and thus lower gas uptake than COP-9.

In DFT calculations, there were cases that included both $CO_2$ and $N_2$ coexisting cases on the top of determined active sites for both the COPs. When COP-9-CN AIM cases were observed, there were no strong interactions for COP9 — $N_2$ recorded, thus these calculations yielded with only COP-9 – $CO_2$ interactions. On the other hand, COP-10-CN cases resulted more balanced interaction distribution including interactions both with $CO_2$ and $N_2$. Highest values of ρ and $\nabla^2\rho$ amongst the other studied cases were calculated at COP-9-CN-p1 for BCP#4 (0.00081564 a.u. and 0.0133556 a.u. respectively); whereas highest values of the

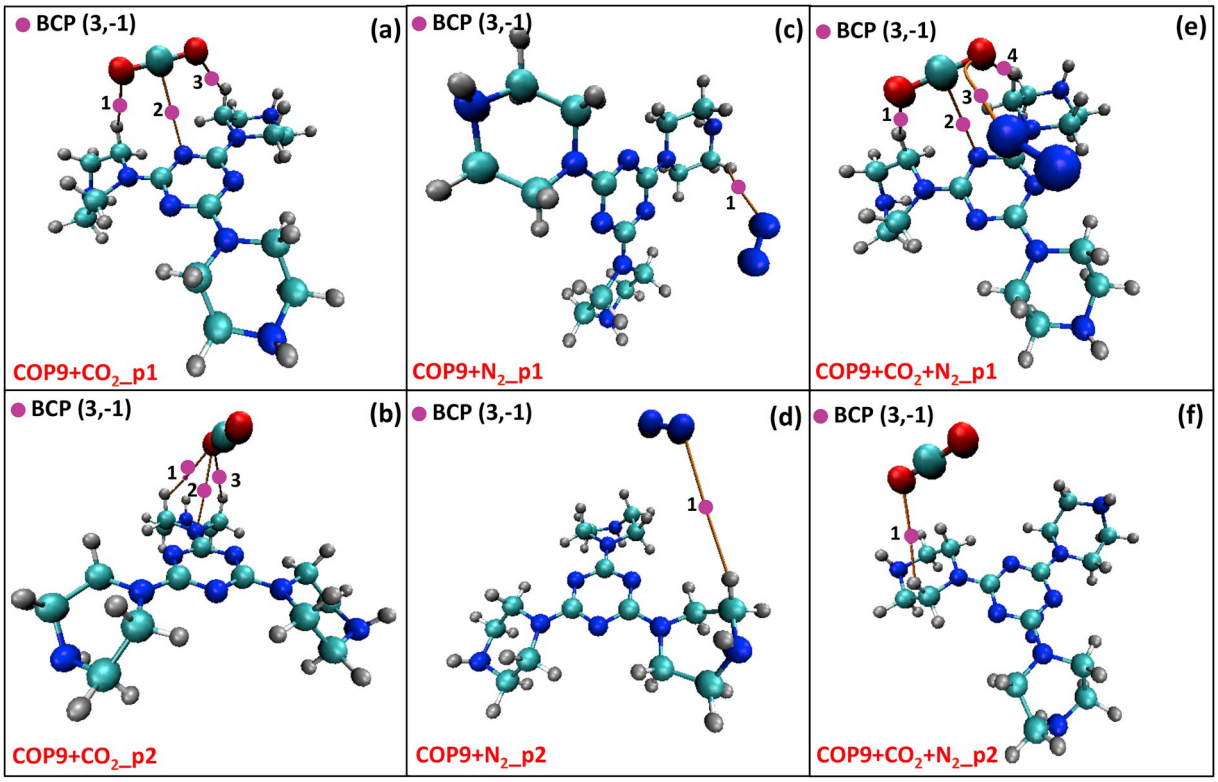


**Fig. 6.** Atom in Molecule (AIM) analysis of COP-9 interactions and bond critical points (BCP) involving COP-9 + $CO_2$, COP-9 + $N_2$ and COP-9 + $CO_2$ + $N_2$ systems. (a) COP-9 + $CO_2$ at position (p) p1, (b) COP-9 + $CO_2$ at p2, (c) COP-9 + $N_2$ at p1, (d) COP-9 + $N_2$ at p2, (c) COP-9 + $CO_2$ + $N_2$ at p1, (d) COP-9 + $CO_2$ + $N_2$ at p2 (p1 and p2 are explained in Scheme 2). Electron density (ρ) and Laplacian of electron density ($\nabla^2\rho$) for COP-9 + $CO_2$ + $N_2$ BCPs are reported separately in Table S1.

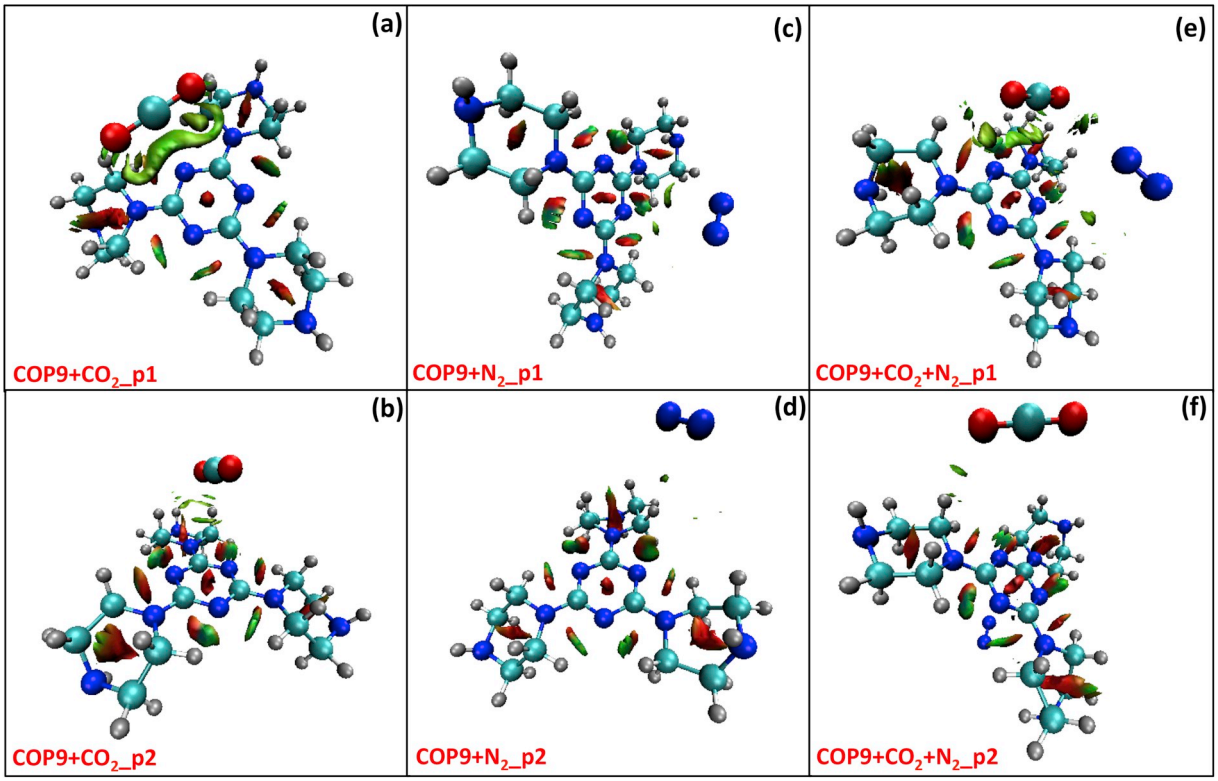


**Fig. 7.** Reduced Density Gradient (RDG) iso-surfaces (green or green-brown color indicates van der Waals interactions) are shown for: (a) COP-9 + $CO_2$ at position (p) p1, (b) COP-9 + $CO_2$ at p2, (c) COP-9 + $N_2$ at p1, (d) COP-9 + $N_2$ at p2, (e) COP-9 + $CO_2$ + $N_2$ at p1, (f) COP-9 + $CO_2$ + $N_2$ at p2 (p1 and p2 are explained in Scheme 2). (For interpretation of the references to color in this figure legend, the reader is referred to the Web version of this article.)

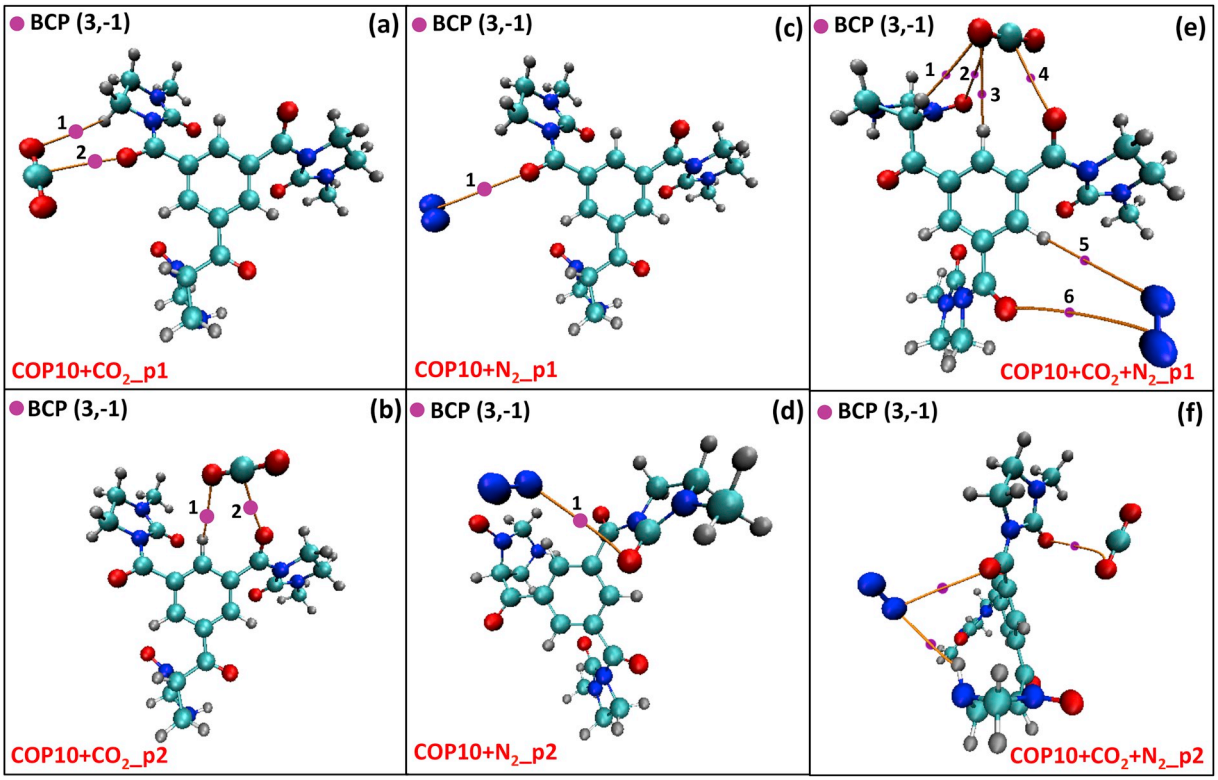


**Fig. 8.** Atom in Molecule (AIM) analysis of COP-10 interactions and bond critical points (BCP) involving COP-10 + $CO_2$, COP-10 + $N_2$ and COP-9 + $CO_2$ + $N_2$ systems. (a) COP-10 + $CO_2$ at position (p) p1, (b) COP-10 + $CO_2$ at p2, (c) COP-10 + $N_2$ at p1, (d) COP-10 + $N_2$ at p2, (c) COP-10 + $CO_2$+$N_2$ at p1, (d) COP-10 + $CO_2$+$N_2$ at p2 (p1 and p2 are explained in Scheme 2). Electron density (ρ) and Laplacian of electron density ($\nabla^2\rho$) for COP-10 + $CO_2$ + $N_2$ BCPs are reported separately in Table S1.

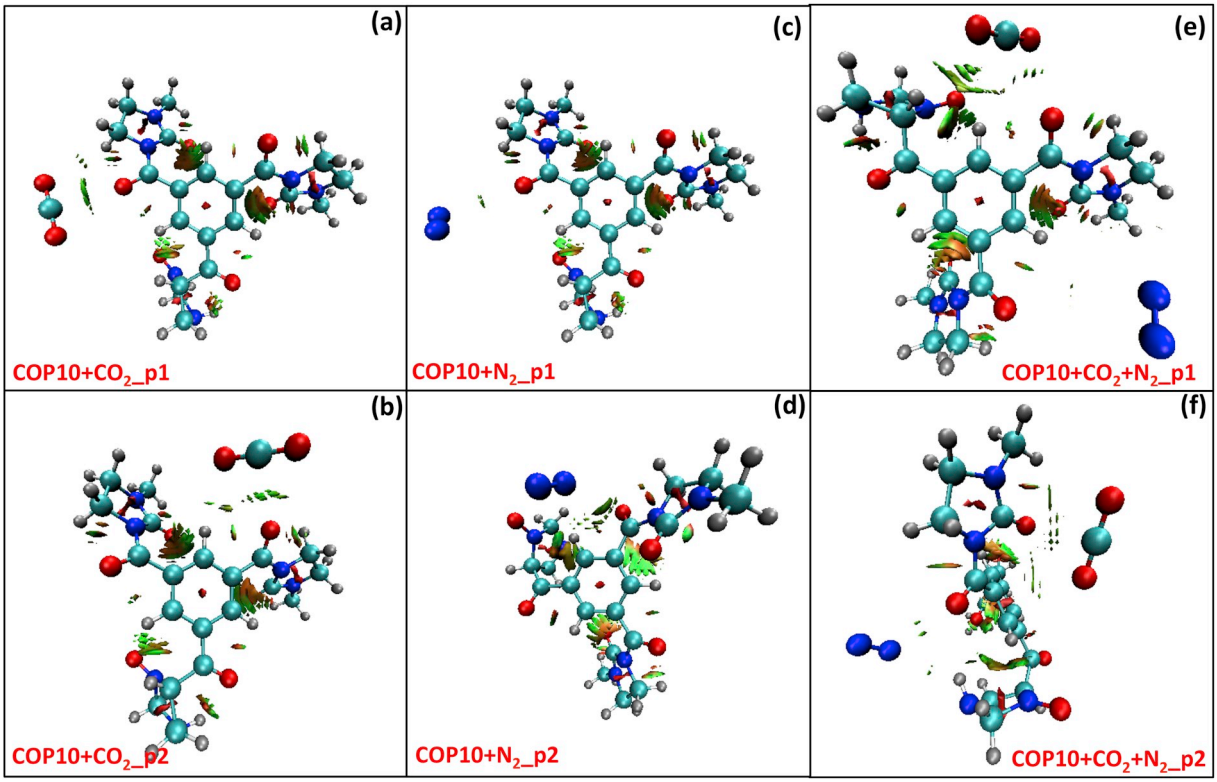


**Fig. 9.** Reduced Density Gradient (RDG) iso-surfaces (green or green-brown color indicates van der Waals interactions) are shown for: (a) COP-9 + $CO_2$ at position (p) p1, (b) COP-10 + $CO_2$ at p2, (c) COP-10 + $N_2$ at p1, (d) COP-10 + $N_2$ at p2, (e) COP-10 + $CO_2$+$N_2$ at p1, (f) COP-10 + $CO_2$+$N_2$ at p2 (p1 and p2 are explained in Scheme 2). (For interpretation of the references to color in this figure legend, the reader is referred to the Web version of this article.)

same quantities for COP-10 were calculated at COP-10-p1 for BCP#4 (0.00115502 a.u. and 0.0215073 a.u. respectively). These results also confirm the highest $CO_2$ affinity than $N_2$ affinity for both COPs, with COP-10 having superior binging interactions than that of COP-9 and it is also inline with the low-pressure experimental data. For COP−CN DFT AIM calculations, interaction details were observed to be COP-9-CN-p1 for BCP#4 as having highest interaction at O···C(H) sites (Fig. 6) and as for the COP-10-p1 for BCP#4 as the highest interaction was observed at C···C(O) sites (Fig. 8). As per the definition of DFT AIM hydrogen bonding conditions (explained above) calculated values of ρ and $\nabla^2\rho$ are outside of the hydrogen bonding limits and these presented interactions indicating a van der Waals type of interaction between $CO_2$ and COPs structure. Having said that, van der Waals type of interaction also explains experimental findings for adsorption-desorption behaviors and how vacuum readings reaches to same value when pressure is released from the COPs. This behavior makes the studied materials suitable for pressure swing adsorption type of applications for the utilization of these COPs. Moreover, the studied RGD isosurfaces between COPs and $CO_2/N_2$ molecules show effective van der Waals interactions for all the studied cases with green (or green-brown) color indicating van der Waals interactions, which is inline with the DFT AIM findings.

## 4. Conclusion

It can be concluded that two covalently bonded organic polymers COP-9 and COP-10 were prepared from two different core building block monomers and linked with different linking agents. Both COPs material were tested for low and high pressure $CO_2$, $H_2$ and $N_2$ adsorption at three different temperatures. It was found that COP-10 has almost three times larger pore volume than COP-9 and therefore captures slightly larger $CO_2$ than COP-9 at atmospheric pressure and room temperature. Additionally, COP-10 uptakes significantly lower quantity of $N_2$ at atmospheric pressure and room temperature while it becomes almost $N_2$ phobic at high temperature and lower pressure, thus resulting in very good selectivity under these conditions. On the other hand at high pressure, capacity of $CO_2$ uptake is larger for COP-9 in comparison to that of COP-10, since the former uptakes 82 mmol/g while the later captures around 52 mmol/g of $CO_2$ at 200 bars and 308 K. Unlike to low pressure performance, selectivity of both the materials is almost similar at high pressure, while it varies slightly at different temperatures. The better performance of COP-9 at higher pressure suggest that, this material needs further investigation for capture of mixed gases like which can make it capable for large scale application both in pre-combustion and post-combustion systems. Moreover, the sorption properties of two COPs were also studied by using DFT calculations (AIM and RDG methods). The systems containing both $CO_2$, $N_2$ and both $CO_2/N_2$ together were considered at various different interaction sites and the DFT simulations obtained for these cases were analyzed in terms of microscopic structure, intermolecular forces, weak or strong bonding locations and topological behaviours in this manuscript, which reveals the details of how the binding occurs and at which interaction sites.

## Acknowledgements

This work was funded by Junta de Castilla y León (Spain, project BU324U14) and National Research Foundation of Korea NRF-2017M3A7B4042140. We also acknowledge The Foundation of Supercomputing Center of Castile and León (FCSCL, Spain) for providing supercomputing facilities. The statements made herein are solely the responsibility of the authors.

## Appendix A. Supplementary data

Supplementary data to this article can be found online at https://doi.org/10.1016/j.micromeso.2018.12.011.

## References

[1] R.S. Haszeldine, Carbon capture and storage: how green can black Be? Science 325 (2009) 1647.
[2] D. Aaron, C. Tsouris, Separation of CO2 from flue gas: a review, Separ. Sci. Technol. 40 (2005) 321–348.
[3] B. Metz, O. Davidson, H. de Coninck, M. Loos, L. Meyer, Special Report on Carbon Dioxide Capture and Storage, Cambridge Univ. Press, Cambridge, 2005.
[4] Greenhouse Gas (GHG) Emissions, US Environmental Protection Agency, 2017, http://www.epa.gov/ghgemissions.
[5] International Energy Outlook 2016, US Energy Information Administration, 2017, http://www.eia.gov/outlooks.
[6] M.E. Boot-Handford, J.C. Abanades, E.J. Anthony, M.J. Blunt, S. Brandani, N. Mac Dowell, J.R. Fernandez, M.-C. Ferrari, R. Gross, J.P. Hallett, R.S. Haszeldine, P. Heptonstall, A. Lyngfelt, Z. Makuch, E. Mangano, R.T.J. Porter, M. Pourkashanian, G.T. Rochelle, N. Shah, J.G. Yao, P.S. Fennell, Carbon capture and storage update, Energy Environ. Sci. 7 (2014) 130–189.
[7] S. Chu, A. Majumdar, Opportunities and challenges for a sustainable energy future, Nature 488 (2012) 294–303.
[8] U. Ahmed, U. Zahid, Y.S. Jeong, C.-J. Lee, C. Han, IGCC process intensification for simultaneous power generation and CO2 capture, Chem. Eng. Process: Process Intensification 101 (2016) 72–86.
[9] A. Awadallah-F, S. Al-Muhtaseb, Carbon dioxide sequestration and methane removal from exhaust gases using resorcinol–formaldehyde activated carbon xerogel, Adsorption 19 (2013) 967–977.
[10] A.H. Berger, A.S. Bhown, Selection of optimal solid sorbents for CO2 capture based on gas phase CO2 composition, Energy Procedia 63 (2014) 2092–2099.
[11] J.H. Cavka, C.A. Grande, G. Mondino, R. Blom, High pressure adsorption of CO2 and CH4 on Zr-MOFs, Ind. Eng. Chem. Res. 53 (2014) 15500–15507.
[12] J. Chen, L.S. Loo, K. Wang, High-pressure CO2 adsorption on a polymer-derived carbon molecular sieve, J. Chem. Eng. Data 53 (2008) 2–4.
[13] M.A. Gonzalez-Salazar, R.J. Perry, R.-K. Vipperla, A. Hernandez-Nogales, L.O. Nord, V. Michelassi, R. Shisler, V. Lissianski, Comparison of current and advanced post-combustion CO2 capture technologies for power plant applications, Energy Procedia 23 (2012) 3–14.
[14] C. Ekström, F. Schwendig, O. Biede, F. Franco, G. Haupt, G. de Koeijer, C. Papapavlou, P.E. Røkke, Techno-economic evaluations and benchmarking of pre-combustion CO2 capture and oxy-fuel processes developed in the european ENCAP project, Energy Procedia 1 (2009) 4233–4240.
[15] R.S. Haszeldine, Carbon capture and storage: how green can black be? Science 325 (2009) 1647–1652.
[16] J. Wang, L. Huang, R. Yang, Z. Zhang, J. Wu, Y. Gao, Q. Wang, D. O'Hare, Z. Zhong, Recent advances in solid sorbents for CO2 capture and new development trends, Energy Environ. Sci. 7 (2014) 3478–3518.
[17] A.R. Millward, O.M. Yaghi, Metal − Organic frameworks with exceptionally high capacity for storage of carbon dioxide at room temperature, J. Am. Chem. Soc. 127 (2005) 17998–17999.
[18] L. Liu, S.-M. Wang, Z.-B. Han, M. Ding, D.-Q. Yuan, H.-L. Jiang, Exceptionally robust in-based metal–organic framework for highly efficient carbon dioxide capture and conversion, Inorg. Chem. 55 (2016) 3558–3565.
[19] T.M. McDonald, W.R. Lee, J.A. Mason, B.M. Wiers, C.S. Hong, J.R. Long, Capture of carbon dioxide from air and flue gas in the alkylamine-appended metal–organic framework mmen-Mg2(dobpdc), J. Am. Chem. Soc. 134 (2012) 7056–7065.
[20] M. Witman, S. Ling, A. Gladysiak, K.C. Stylianou, B. Smit, B. Slater, M. Haranczyk, Rational design of a low-cost, high-performance metal–organic framework for hydrogen storage and carbon capture, J. Phys. Chem. C 121 (2017) 1171–1181.
[21] W. Morris, B. Leung, H. Furukawa, O.K. Yaghi, N. He, H. Hayashi, Y. Houndonougbo, M. Asta, B.B. Laird, O.M. Yaghi, A combined Experimental − Computational investigation of carbon dioxide capture in a series of isoreticular zeolitic imidazolate frameworks, J. Am. Chem. Soc. 132 (2010) 11006–11008.
[22] J.C. Fisher, R.V. Siriwardane, R.W. Stevens, Zeolite-based process for CO2 capture from high-pressure, moderate-temperature gas streams, Ind. Eng. Chem. Res. 50 (2011) 13962–13968.
[23] J. Kim, L.-C. Lin, J.A. Swisher, M. Haranczyk, B. Smit, Predicting large CO2 adsorption in aluminosilicate zeolites for postcombustion carbon dioxide capture, J. Am. Chem. Soc. 134 (2012) 18940–18943.
[24] G.N. Nikolaidis, E.S. Kikkinides, M.C. Georgiadis, An integrated two-stage P/VSA process for postcombustion CO2 capture using combinations of adsorbents zeolite 13X and Mg-MOF-74, Ind. Eng. Chem. Res. 56 (2017) 974–988.
[25] N.R. Stuckert, R.T. Yang, CO2 capture from the atmosphere and simultaneous concentration using zeolites and amine-grafted SBA-15, Environ. Sci. Technol. 45 (2011) 10257–10264.
[26] M. Vinoba, M. Bhagiyalakshmi, S.K. Jeong, Y. Yoon, II, S.C. Nam, Capture and sequestration of CO2 by human carbonic anhydrase covalently immobilized onto amine-functionalized SBA-15, J. Phys. Chem. C 115 (2011) 20209–20216.
[27] R. Ullah, M. Atilhan, S. Aparicio, A. Canlier, C.T. Yavuz, Insights of CO2 adsorption performance of amine impregnated mesoporous silica (SBA-15) at wide range pressure and temperature conditions, International Journal of Greenhouse Gas Control 43 (2015) 22–32.
[28] M. Atilhan, S. Atilhan, R. Ullah, B. Anaya, T. Cagin, C.T. Yavuz, S. Aparicio, High-pressure methane, carbon dioxide, and nitrogen adsorption on amine-impregnated porous montmorillonite nanoclays, J. Chem. Eng. Data 61 (2016) 2749–2760.
[29] S.D. Kenarsari, D. Yang, G. Jiang, S. Zhang, J. Wang, A.G. Russell, Q. Wei, M. Fan, Review of recent advances in carbon dioxide separation and capture, RSC Adv. 3

(2013) 22739–22773.
[30] J.-K. Sun, M. Antonietti, J. Yuan, Nanoporous ionic organic networks: from synthesis to materials applications, Chem. Soc. Rev. 45 (2016) 6627–6656.
[31] J. Wang, I. Senkovska, M. Oschatz, M.R. Lohe, L. Borchardt, A. Heerwig, Q. Liu, S. Kaskel, Highly porous nitrogen-doped polyimine-based carbons with adjustable microstructures for CO2 capture, J. Mater. Chem. 1 (2013) 10951–10961.
[32] W. Wang, M. Zhou, D. Yuan, Carbon dioxide capture in amorphous porous organic polymers, J. Mater. Chem. 5 (2017) 1334–1347.
[33] Z. Xiang, D. Cao, Porous covalent-organic materials: synthesis, clean energy application and design, J. Mater. Chem. 1 (2013) 2691–2718.
[34] R. Ullah, M. Atilhan, B. Anaya, S. Al-Muhtaseb, S. Aparicio, H. Patel, D. Thirion, C.T. Yavuz, Investigation of ester- and amide-linker-based porous organic polymers for carbon dioxide capture and separation at wide temperatures and pressures, ACS Appl. Mater. Interfaces 8 (2016) 20772–20785.
[35] H. Furukawa, O.M. Yaghi, Storage of hydrogen, methane, and carbon dioxide in highly porous covalent organic frameworks for clean energy applications, J. Am. Chem. Soc. 131 (2009) 8875–8883.
[36] N. Hedin, L. Andersson, L. Bergström, J. Yan, Adsorbents for the post-combustion capture of CO2 using rapid temperature swing or vacuum swing adsorption, Appl. Energy 104 (2013) 418–433.
[37] N.B. McKeown, P.M. Budd, Polymers of intrinsic microporosity (PIMs): organic materials for membrane separations, heterogeneous catalysis and hydrogen storage, Chem. Soc. Rev. 35 (2006) 675–683.
[38] A. Modak, A. Bhaumik, Porous carbon derived via KOH activation of a hypercrosslinked porous organic polymer for efficient CO2, CH4, H2 adsorptions and high CO2/N2 selectivity, J. Solid State Chem. 232 (2015) 157–162.
[39] M.G. Plaza, C. Pevida, A. Arenillas, F. Rubiera, J.J. Pis, CO2 capture by adsorption with nitrogen enriched carbons, Fuel 86 (2007) 2204–2212.
[40] E. Deniz, F. Karadas, H.A. Patel, S. Aparicio, C.T. Yavuz, M. Atilhan, A combined computational and experimental study of high pressure and supercritical CO2 adsorption on Basolite MOFs, Microporous Mesoporous Mater. 175 (2013) 34–42.
[41] S. Adams, P. de Castro, P. Echenique, J. Estrada, M.D. Hanwell, P. Murray-Rust, P. Sherwood, J. Thomas, J.A. Townsend, The quixote project: collaborative and open quantum chemistry data management in the internet age, J. Cheminf. 3 (2011).
[42] F. Neese, The ORCA program system, Wiley Interdisciplinary Reviews: Computational Molecular Science 2 (2012) 73–78.
[43] C. Lee, W. Yang, R.G. Parr, Development of the Colle-Salvetti correlation-energy formula into a functional of the electron density, Phys. Rev. B 37 (1988) 785–789.
[44] A.D. Becke, Density-functional exchange-energy approximation with correct asymptotic behavior, Phys. Rev. 38 (1988) 3098–3100.
[45] S. Grimme, J. Antony, S. Ehrlich, H. Krieg, A consistent and accurate ab initio parametrization of density functional dispersion correction (DFT-D) for the 94 elements H-Pu, J. Chem. Phys. 132 (2010) 154104.
[46] R.F.W. Bader, Atoms in Molecules: a Quantum Theory, Oxford University Press, 1990.
[47] T. Lu, F. Chen, Multiwfn: a multifunctional wavefunction analyzer, J. Comput. Chem. 33 (2012) 580–592.
[48] G. Saleh, C. Gatti, L. Lo Presti, Non-covalent interaction via the reduced density gradient: independent atom model vs experimental multipolar electron densities, Computational and Theoretical Chemistry 998 (2012) 148–163.
[49] A. Zupan, J.P. Perdew, K. Burke, M. Causà, Density-gradient analysis for density functional theory: application to atoms, Int. J. Quant. Chem. 61 (1997) 835–845.
[50] A. Zupan, K. Burke, M. Ernzerhof, J.P. Perdew, Distributions and averages of electron density parameters: explaining the effects of gradient corrections, J. Chem. Phys. 106 (1997) 10184–10193.
[51] Y. Belmabkhout, V. Guillerm, M. Eddaoudi, Low concentration CO2 capture using physical adsorbents: are metal–organic frameworks becoming the new benchmark materials? Chem. Eng. J. 296 (2016) 386–397.
[52] R. Veneman, W. Zhao, Z. Li, N. Cai, D.W.F. Brilman, Adsorption of CO2 and H2O on supported amine sorbents, Energy Procedia 63 (2014) 2336–2345.
[53] S. Zulfiqar, M.I. Sarwar, C.T. Yavuz, Melamine based porous organic amide polymers for CO2 capture, RSC Adv. 4 (2014) 52263–52269.
[54] M. Worzakowska, TG/FTIR/QMS studies of long chain esters of geraniol, J. Anal. Appl. Pyrol. 110 (2014) 181–193.
[55] Z. Xiang, X. Zhou, C. Zhou, S. Zhong, X. He, C. Qin, D. Cao, Covalent-organic polymers for carbon dioxide capture, J. Mater. Chem. 22 (2012) 22663–22669.
[56] J.Y. Jung, F. Karadas, S. Zulfiqar, E. Deniz, S. Aparicio, M. Atilhan, C.T. Yavuz, S.M. Han, Limitations and high pressure behavior of MOF-5 for CO2 capture, Phys. Chem. Chem. Phys. 15 (2013) 14319–14327.
[57] H.A. Patel, F. Karadas, A. Canlier, J. Park, E. Deniz, Y. Jung, M. Atilhan, C.T. Yavuz, High capacity carbon dioxide adsorption by inexpensive covalent organic polymers, J. Mater. Chem. 22 (2012) 8431–8437.
[58] S. Zulfiqar, S. Awan, F. Karadas, M. Atilhan, C.T. Yavuz, M.I. Sarwar, Amidoxime porous polymers for CO2 capture, RSC Adv. 3 (2013) 17203–17213.
[59] S. Zulfiqar, F. Karadas, J. Park, E. Deniz, G.D. Stucky, Y. Jung, M. Atilhan, C.T. Yavuz, Amidoximes: promising candidates for CO2 capture, Energy Environ. Sci. 4 (2011) 4528–4531.
[60] H.A. Patel, F. Karadas, J. Byun, J. Park, E. Deniz, A. Canlier, Y. Jung, M. Atilhan, C.T. Yavuz, Highly stable nanoporous sulfur-bridged covalent organic polymers for carbon dioxide removal, Adv. Funct. Mater. 23 (2013) 2270–2276.
[61] C.R. Mason, L. Maynard-Atem, K.W.J. Heard, B. Satilmis, P.M. Budd, K. Friess, M. Lanč, P. Bernardo, G. Clarizia, J.C. Jansen, Enhancement of CO2 affinity in a polymer of intrinsic microporosity by amine modification, Macromolecules 47 (2014) 1021–1029.
[62] N.B. McKeown, P.M. Budd, Exploitation of intrinsic microporosity in polymer-based materials, Macromolecules 43 (2010) 5163–5176.
[63] J.U. Keller, R. Staudt, Adsorption Isotherms, Gas Adsorption Equilibria: Experimental Methods and Adsorptive Isotherms, Springer US, Boston, MA, 2005, pp. 359–413.
[64] R. Ullah, M. Atilhan, A. Diab, E. Deniz, S. Aparicio, C.T. Yavuz, Synthesis, characterization and evaluation of porous polybenzimidazole materials for CO2 adsorption at high pressures, Adsorption (2016) 1–14.
[65] D. Bhattacharyya, D.C. Miller, Post-combustion CO2 capture technologies — a review of processes for solvent-based and sorbent-based CO2 capture, Current Opinion in Chemical Engineering 17 (2017) 78–92.
[66] D. Chen, S. Gu, Y. Fu, Y. Zhu, C. Liu, G. Li, G. Yu, C. Pan, Tunable porosity of nanoporous organic polymers with hierarchical pores for enhanced CO2 capture, Polym. Chem. 7 (2016) 3416–3422.
[67] Z. Bao, L. Yu, Q. Ren, X. Lu, S. Deng, Adsorption of CO2 and CH4 on a magnesium-based metal organic framework, J. Colloid Interface Sci. 353 (2011) 549–556.
[68] H. Pan, J.A. Ritter, P.B. Balbuena, Examination of the approximations used in determining the isosteric heat of adsorption from the Clausius − Clapeyron equation, Langmuir 14 (1998) 6323–6327.
[69] H. Roohi, A.-R. Nowroozi, E. Anjomshoa, H-bonded complexes of uracil with parent nitrosamine: a quantum chemical study, Computational and Theoretical Chemistry 965 (2011) 211–220.